Supplementary Information: Two octave supercontinuum generation in a non-silica graded-index multimode fiber

Zahra Eslami[1], Lauri Salmela[1], Adam Filipkowski[2,3], Dariusz Pysz[2], Mariusz Klimczak[3], Ryszard Buczynski[2,3], John M. Dudley[4], and Goëry Genty[1,*]

[1]Photonics Laboratory, Physics Unit, Tampere University, 33014 Tampere, Finland
[2]Łukasiewicz Research Network – Institute of Microelectronics and Photonics, Al. Lotników 32/46, 02-668 Warsaw, Poland
[3]University of Warsaw, Faculty of Physics, Pasteura 5, 02-093 Warsaw, Poland.
[4]Institut FEMTO-ST, Université Bourgogne Franche-Comté CNRS UMR 6174, 25000 Besançon, France
[*]goery.genty@tuni.fi

Critical power for self-focusing

For sufficiently large peak power, the Kerr nonlinearity can act as a nonlinear lens and lead to self-focusing of the beam [1,2] and catastrophic collapse [3–5]. The critical value of injected power P_{cr} for which Kerr-induced self-focusing occurs can be estimated from [6]

$$P_{\mathrm{cr}} = \alpha \frac{\lambda_0^2}{4\pi n_{co} n_2}, \tag{1}$$

where λ_0 is the central wavelength of the beam, n_{co} the core refractive index of the fiber, n_2 the nonlinear refractive index, and $\alpha \approx 1.9$ for a Gaussian beam. For our fiber, the corresponding critical power value is $P_{\mathrm{cr}} = 1.2$ MW. In our experiments (and numerical simulations), the peak power value is always below this limit due to the significant attenuation resulting from leakage to the cladding in the very first cm of propagation, the rapid temporal broadening when pumping in the normal dispersion regime at 1700 nm and reduced OPA power in the anomalous dispersion regime at 2500 nm. This is also confirmed by the numerical simulation shown in Fig. 5 of the main manuscript.

Effect of Raman response on propagation dynamics

In order to study the effect of the Raman response on the propagation dynamics, we have performed 3+1D GNLSE numerical simulations with and without the Raman contribution included. The Raman response was modeled as a delayed response using the conventional form

$$h_R(T) = f_R \left(\tau_1^2 + \tau_2^2\right) \tau_1 e^{-\frac{T}{\tau_2}} \sin(T/\tau_2), \tag{2}$$

with the values τ_1=5.5 fs, τ_2=32 fs, and $f_R = 0.05$ corresponding to those measured for PBG glass [7]. The result of the comparison is shown in Fig. 1 where we plot the generated supercontinuum (SC) spectra with (right) and without (left) the Raman term included in the simulations, both for a pump wavelength at 1700 nm in the normal dispersion regime (top row) and 2500 nm in the anomalous dispersion regime (bottom row). One can see that, independently of the pumping regime (normal or anomalous), the Raman response has a negligible effect on the generated SC spectra. This can be attributed to the relatively low Raman gain of the PBG glasses as compared to silica and the short length of the fiber (20 cm) which limits Raman-induced dynamics.

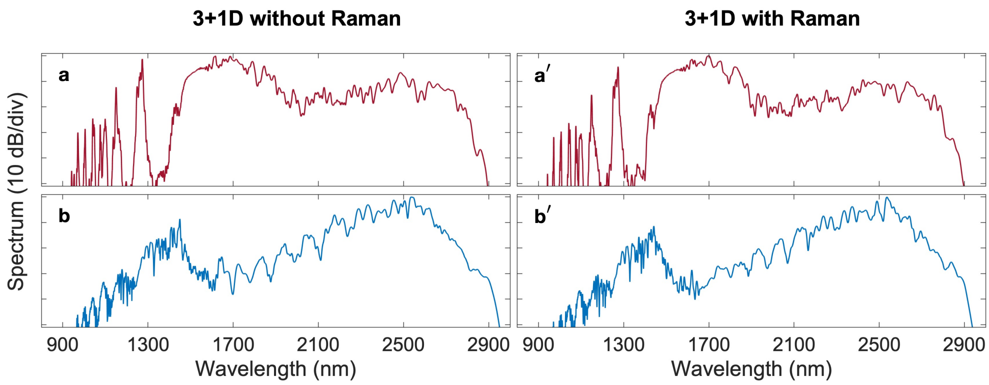

Supplementary Figure 1: Effect of Raman gain on propagation dynamics. Left column: 3+1D simulations without the Raman response included. Right column: 3+1D simulations with the Raman response included. Top row: Pump wavelength at 1700 nm, P_p =700 kW. Bottom row: Pump wavelength at 2500 nm, P_p =450 kW. The corresponding spectra are generated using identical noise seeds in the spectral and spatial domains.

3+1D and 1+1D modeling comparison

We performed a numerical comparison between the time-consuming 3+1D GNLSE model and the simplified significantly faster 1+1D GNLSE model where the self-imaging dynamics are accounted for by a periodic change of the effective area [8]. In the 1+1D approach, the beam spot size (1/e intensity radius) along the fiber can be written as

$$a^2(z) = a_0^2[\cos^2(\sqrt{g}z) + C\sin^2(\sqrt{g}z)], \tag{3}$$

where a_0 is the input beam radius (1/e intensity waist), $g = 2\Delta/R^2$, $\Delta = (n_{co}^2 - n_{cl}^2)/2n_{co}^2$ is the relative refractive index difference, and $C = (1-p)/(\beta_0 a_0^4 g) \approx 1/\beta_0 a_0^4 g$ under stationary self-imaging conditions. The nonlinear coefficient γ of the fiber can be calculated through the z-dependent effective area as

$$\gamma(z) = \frac{\omega_0 n_2}{cA_{\text{eff}}(z)} = \frac{\omega_0 n_2}{2\pi c a^2(z)}, \tag{4}$$

where $a(z)$ is the beam size from Eq. 3. We consider an input beam size of 25 μm (1/e^2 intensity radius), fiber core radius of R = 40 μm, and nonlinear refractive index n_2 of 1.92×10^{-19} m^{2}W^{-1}. The simulations use up to 65536 spectral/temporal grid points with temporal window size of 80 ps, spectral resolution of 12.5 GHz and a step size of 6.7 μm (30,000 steps). Shot noise is added via one-photon-per-mode with random phase in the frequency domain. In the comparison, no input phase noise is added to the spatial amplitude distribution for the 3+1D model. Figure 2 compares the average SC spectrum for increasing input peak power and a pump wavelength of 2500 nm. The 3+1D and 1+1D spectra are convolved with a super Gaussian filter with 2 nm bandwidth and averaged over 10 and 50 realizations, respectively. In agreement with previous studies [8, 9], we see relatively good correspondence between the two models. The 1+1D model reproduces the main features and can be conveniently used to verify the propagation dynamics that leads to the supercontinuum development while saving considerable computing time and memory, and this is the model we use in the Supplementary Movies showing the time-frequency spectrogram evolution along propagation. Note that including spatial input phase noise in the 3+1D model (as was done for the simulation results shown in the main manuscript) leads to a fraction of the energy to leak to cladding and a reduced supercontinuum spectral bandwidth as compared to when spatial noise is not added (and also the 1+1D model). This can be compensated for when spatial noise is added by adjusting the injected peak power to yield an output energy identical to the noiseless case.

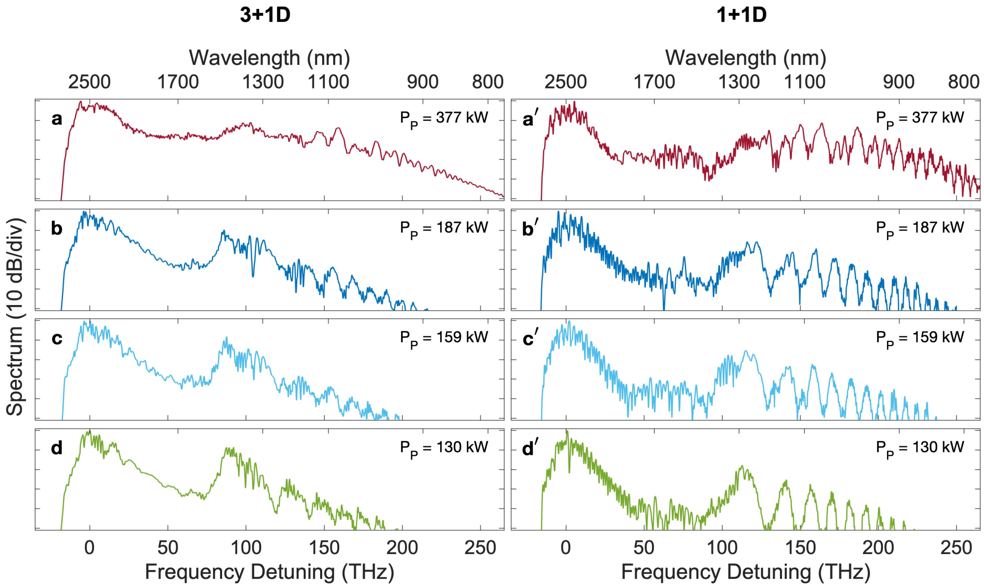

Supplementary Figure 2: 3+1D (a-d) and 1+1D (a' to d') numerical simulation of supercontinuum spectra as a function of launched peak power a) $P_P = 377$ kW b) $P_P = 187$ kW c) $P_P = 159$ kW d) $P_P = 130$ kW (for a fixed length of 20 cm and pump wavelength of 2500 nm). The injected beam was of a clean Gaussian pulse without phase noise for the 3+1D simulations. The spectra are averaged over 10 and 50 realizations for the 3+1D and 1+1D simulations, respectively.

Power dependence of the supercontinuum spectrum for 2500 nm pump wavelength

We characterized the supercontinuum spectrum generated as a function of injected peak power when the OPA was tuned to 2500 nm in the anomalous dispersion regime of the fiber. The results are shown in Fig. 3. In this case the generating mechanism is triggered by higher-order soliton compression and fission with multiple dispersive waves emission that are manifested as discrete spectral components in the normal dispersion region. This scenario is confirmed by the simulated spectrogram evolution along propagation (using the simplified 1+1D model) and shown in the Supplementary Movie 2. Note that unlike the geometric parametric instabilities observed in the normal dispersion regime and that are seeded by noise, the multiple dispersive waves emission mechanism is a coherent process seeded by the spectral components of the compressed soliton spectrum [10,11]. The theoretical location of the dispersive waves angular frequencies ω_m where m is an integer ($m = 0, \pm 1, \pm 2, \pm 3...$) can be determined from the following phasematching condition [12,13]:

$$\sum_{k\geq 2} \frac{\beta_k}{k!} (\omega_m - \omega_0)^2 - \frac{\gamma P_p}{2} = \frac{2\pi m}{z_p} \tag{5}$$

where β_k represent the Taylor series expansion dispersion coefficients at the pump angular frequency ω_0, γ is the nonlinear coefficient and P_p the peak power. $z_p = \pi R/\sqrt{2\Delta}$ is the self-imaging period with $\Delta = (n_{co} - n_{cl})/n_{co}$ and R the fiber core radius. For our fiber at 2500 nm $n_{co} = 1.872$, $n_{cl} = 1.854$, $\Delta = 0.0096$, R=40 µm, $z_p = 0.91$ mm, $\gamma = 1.95 \times 10^{-19}$ m^{-1}W^{-1}. At low power values, the dispersive waves are clearly apparent in the spectrum and their frequencies are in good agreement with the theoretical predictions indicated by the vertical dashed lines. The residual discrepancy arises from cross-phase modulation with the solitonic components inducing a shift in the dispersive waves position. In principle and in contrast to dispersive waves emitted in single-mode fibers, the periodic perturbation arising from self-imaging can produce dispersive waves components both on the short and long wavelengths side of the spectrum. However, here the long wavelengths components are not observed due to the strong glass absorption beyond 2800 nm. As the peak power is increased, the number of dispersive waves components increases. For the largest injected peak power value, the input soliton number $N = \sqrt{\gamma P_p T_0^2/\beta_2} = 14$ (T_0=$T_{\mathrm{FWHM}}/1.665$) and interactions via cross-phase modulation between the large number of solitons ejected from the fission process and the dispersive waves leads to the merging of the latter yielding a quasi-continuous supercontinuum spectrum.

Spectrogram animations

The Supplementary Movies show the numerically simulated spectrogram evolution as a function of propagation distance for a pump wavelength at 1700 nm and 2500 nm, based on the 1+1D model. The spectrogram is calculated as

$$S(\omega, \tau, z) = \left| \int_{-\infty}^{+\infty} g\,(T - \tau)\, E(z, T) \exp(-i\omega T) dT \right|^2 \tag{6}$$

where $E(z, T)$ represents the time-dependent complex electric field at propagation distance z and $g(T - \tau)$ is a gate function with delay value τ. The spectrogram animation shows the spectra of a series of time-gated portions of the field as a function of propagation coordinate. In our calculation of the spectrogram, we used a hyperbolic-secant gate function of 100 fs duration (full width at half maximum).

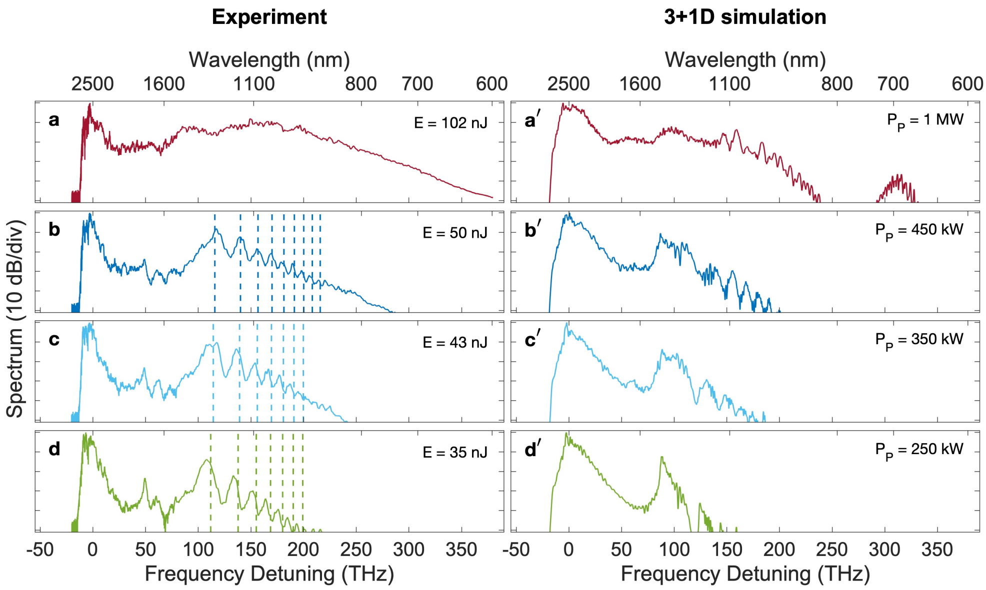

Supplementary Figure 3: Experimental (a-d) and numerical (a' to d') supercontinuum spectra generated in 20 cm of the fiber for a pump wavelength at 2500 nm and increasing peak power. The peak power (P_p) in the simulations is adjusted to match the output energy (E) measured in the experiments. The simulated spectra are averaged over 10 realizations with different spectral and spatial noise seeds. The vertical dashed lines indicate the theoretical frequency of the radiated dispersive waves. Note that in calculating the wavelength of the dispersive waves we have used the peak power at the point of maximum compression taken from the numerical simulations.

References

[1] R. Y. Chiao, E. Garmire, C. H. Townes, *Physical Review Letters* **1964**, *13*, 15 479.

[2] P. Kelley, *Physical Review Letters* **1965**, *15*, 26 1005.

[3] A. L. Gaeta, *Physical Review Letters* **2000**, *84*, 16 3582.

[4] M. R. Vaziri, *Laser Physics* **2013**, *23*, 10 105401.

[5] K. Moll, A. L. Gaeta, G. Fibich, *Physical Review Letters* **2003**, *90*, 20 203902.

[6] G. Fibich, A. L. Gaeta, *Optics Letters* **2000**, *25* 335.

[7] G. Sobon, M. Klimczak, J. Sotor, K. Krzempek, D. Pysz, R. Stepien, T. Martynkien, K. M. Abramski, R. Buczynski, *Optical Materials Express* **2014**, *4*, 1 7.

[8] M. Conforti, C. M. Arabi, A. Mussot, A. Kudlinski, *Optics Letters* **2017**, *42*, 19 4004.

[9] L. G. Wright, S. Wabnitz, D. N. Christodoulides, F. W. Wise, *Physical Review Letters* **2015**, *115*, 22 223902.

[10] N. Akhmediev, M. Karlsson, *Physical Review A* **1995**, *51*, 3 2602.

[11] M. Erkintalo, Y. Xu, S. Murdoch, J. M. Dudley, G. Genty, *Physical Review Letters* **2012**, *109*, 22 223904.

[12] M. Conforti, S. Trillo, A. Mussot, A. Kudlinski, *Scientific Reports* **2015**, *5*, 1 1.

[13] M. Eftekhar, H. Lopez-Aviles, F. Wise, R. Amezcua-Correa, D. Christodoulides, *Communications Physics* **2021**, *4*, 1 1.